International Journal of Biological Macromolecules 337 (2026) 149435

Contents lists available at ScienceDirect

International Journal of Biological Macromolecules

journal homepage: www.elsevier.com/locate/ijbiomac

Evaluating the therapeutic role of salvianolic acid A on pancreatic cancer cells through interaction with the intrinsically disordered protein NUPR1

María Gabriela Álvarez-Rodríguez [a,1], Matías Estaras [b,1], Felipe Hornos [a], Bruno Rizzuti [c,d], Patricia Santofimia-Castaño [b], Juan L. Iovanna [b,*], José L. Neira [a,d,**]

[a] IDIBE, Edificio Torregaitán, Universidad Miguel Hernández, Avenida del Ferrocarril s/n, 03202, Elche, Alicante, Spain
[b] Centre de Recherche en Cancérologie de Marseille (CRCM), INSERM U1068, CNRS UMR 7258, Aix-Marseille Université and Institut Paoli-Calmettes, Parc Scientifique et Technologique de Luminy, 13288, Marseille, France
[c] CNR-NANOTEC, SS Rende (CS), Department of Physics, University of Calabria, 87036, Rende, Italy
[d] Instituto de Biocomputación y Física de Sistemas Complejos (BIFI), Universidad de Zaragoza, 50018, Zaragoza, Spain.

ARTICLE INFO

Keywords:
Intrinsically disordered proteins
Protein-drug interactions
Cell assays
Natural compounds
Molecular docking

ABSTRACT

The nuclear protein 1 (NUPR1) is an intrinsically disordered protein (IDP) involved in stress processes in the cell. We have been developing, by using organic chemistry, several small molecules which hamper *in vitro* and in cell-based assays NUPR1 biomolecular interactions by targeting its two hot-spots around Ala33 and Thr68. In this work, we used a natural compound, salvianolic acid A (SAA), to target NUPR1. SAA has anti-cancer and anti-inflammatory properties. Binding *in vitro* was monitored by using fluorescence, isothermal titration calorimetry (ITC) and nuclear magnetic resonance (NMR); the affinity was in the low micromolar range, as shown by fluorescence and ITC. The NMR spectra of NUPR1, in the absence and in the presence of SAA, indicated that binding involved several polypeptide patches of NUPR1, as well as its hot-spots; however, the binding did not alter the disordered nature of the protein. Moreover, molecular docking simulations provided a model of the binding at the atomic level. Results of proliferation cellular assays with MIA PaCa-2 cells indicated that the IC_{50} was ~20 μM, confirming the affinity values found by fluorescence and ITC. SAA was also capable of inhibiting the formation of stress granules (SGs) triggered by NUPR1. Our work shows that a plant-derived molecule can target an IDP involved in cancer, with affinities in the low micromolar range. Our model compound can hamper the pathological state (SG formation) triggered by this IDP, and indicates that the search for potential inhibitors of disordered proteins could be further extended to bioactive natural compounds.

1. Introduction

The nuclear protein 1 (NUPR1) is an 82-residue-long, intrinsically disordered protein (IDP) with several functions, ranging from being a transcription factor to a regulator of apoptosis [1–3]. Its interactome involves molecules from different sources: from other proteins to saccharides, lipids, and nucleic acids [4–8]. NUPR1 is specifically overexpressed in pancreatic ductal adenocarcinoma (PDAC): in fact, it is involved in the incidence, development and metastasis of PDAC [3,9,10]. Therefore, it can be considered as a potential therapeutic target for this serious illness [1–3]. Due to its intrinsically disordered nature, finding inhibitors targeting NUPR1 is challenging by using traditional drug design, since common structure-based approaches cannot be employed. We have used a mid-throughput experimental

Abbreviations: BMRB, Biomagnetic Resonance Bank; DMEM, Dulbecco's modified Eagle's medium; DMSO, di-methyl sulfoxide; FBS, fetal bovine serum; G3BP, Ras GTPase-activating protein-binding protein; hPScs, human pancreatic stellate cells; HSQC, heteronuclear single quantum coherence; IDP, intrinsically disordered protein; ITC, isothermal titration calorimetry; LLPS, liquid-liquid phase separation; MD, molecular dynamics; MMP9, matrix metalloproteinase-9; mTORC, mammalian target of rapamycin kinase; NMR, nuclear magnetic resonance; NUPR1, nuclear protein 1; PDAC, pancreatic ductal adenocarcinoma; PPI, protein-protein interaction; ROS, reactive oxygen species; SAA, salvianolic acid A; SD, standard deviation; SG, stress granule; TCM, traditional Chinese medicine; TFP, trifluoperazine; TSP, 3-(trimethylsilyl)propionic-2,2,3,3-d_4 acid sodium salt.

* Corresponding author.
** Correspondence to: J. L. Neira, IDIBE, Edificio Torregaitán, Universidad Miguel Hernández, Avda. del Ferrocarril s/n, 03202, Elche, Alicante, Spain.
E-mail addresses: juan.iovanna@inserm.fr (J.L. Iovanna), jlneira@umh.es (J.L. Neira).
[1] These two authors contributed equally to this work.

https://doi.org/10.1016/j.ijbiomac.2025.149435
Received 21 August 2025; Received in revised form 30 November 2025; Accepted 1 December 2025
Available online 3 December 2025

screening to repurpose the antipsychotic drug trifluoperazine (TFP) as a NUPR1 inhibitor [11–14]. TFP has been improved *in silico*, and the additional organic synthesis of several new compounds, together with the use of an array of biological, biochemical and biophysical methods, has led to the development of ZZW-115. The ZZW-115 compound as an inhibitor of NUPR1 protein-protein interactions (PPIs), led to the suppression of tumor cell growth both in cell-based assays and *in vivo* [12,15,16]. In addition, ZZW-115 hampers stress granules (SGs) formation; SGs are needed in some of the NUPR1 functions [17]. SGs are membrane less organelles, caused by liquid-liquid phase separation (LLPS), whose formation is triggered by cellular stress environmental conditions and in most cases formed by RNA and RNA-binding proteins (see [17] and references therein). However, ZZW-115 has side effects during preclinical studies [18], and then, it is necessary to identify, by using natural resources, or alternatively *in silico* and synthetic techniques, new NUPR1 inhibitors. For instance, we have started exploring how new synthetic organosilicon molecules are capable of binding to NUPR1, and they are interfering with its PPIs within the cell [19].

In recent years, some of the compounds used in Traditional Chinese Medicine (TCM) have been employed as alternative therapies to conventional cancer treatments [20]. Preclinical and clinical studies have shown the usefulness of TCM in alleviating cancer-related symptoms, enhancing patient quality of life, and potentially improving therapeutic outcomes when incorporated into multimodal treatment regimens [20]. Among the bioactive compounds derived from Chinese medicinal herbs, polyphenols are important due to their beneficial medical properties with minimal toxicity [21]. Polyphenols encompass phenolic acids, flavonoids [22], tannins and stilbenoids, all of which are abundantly found in medicinal herbs and plants [23]. Salvianolic acid A (SAA) is a stilbenoid (Scheme 1), that is isolated from the radix of *Salvia miltiorrhiza*, as well as from the root extract of *Salvia yunnanensis*. SAA is a water-soluble compound with anti-inflammatory [24], anti-cancer [25] and anti-oxidant [26] properties. In general, due to its large availability, the roots of *Salvia miltiorrhiza* are being utilized for several years now in TCM as a treatment for cancer [27]. Therefore, all these applications and the fact that a few natural compounds have been used as drugs against IDPs [28,29], prompted us to employ SAA against NUPR1.

In this work, we investigated the binding between NUPR1 and SAA *in vitro*, *in silico* and in cell-based assays. At the best of our knowledge, this would be the first use of a plant-derived, natural compound against an IDP involved in cancer development, although natural compounds have been used to target IDPs implicated in neurodegenerative diseases mainly to hamper intermolecular interactions [28,29]. We obtained an affinity constant for the binding between wild-type NUPR1 and SAA in the range of 20–30 μM, as shown by fluorescence and ITC. Interaction between wild-type NUPR1 and SAA, as monitored by 2D ^{1}H-^{15}N HSQC NMR, involved a decrease of the intensity of most of the protein signals, including those of the two hot-spots. Furthermore, molecular docking simulations provided a model of the NUPR1/SAA complex that agreed with the presence of two binding hot-spots on the protein. Studies with several pancreatic cancer cell lines showed that SAA had a cytotoxic effect, which did not depend on the presence of NUPR1 in the cell lines, as shown by experiments with Panc-1 NUPR1 KO ones. Nevertheless, the treatment with SAA disrupted SGs formation, triggered by the presence of NUPR1. Although the exact mechanism by which this disruption happens is not yet fully known, these results open the possibility of using this natural product as an agent modulating this important type of supramolecular structures for survival of cancer cells.

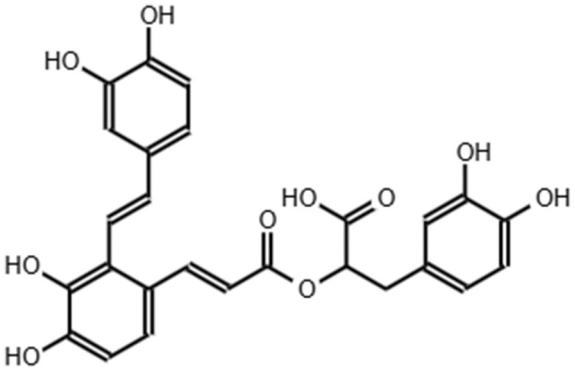

Scheme 1. Structure of salvianolic acid A.

2. Materials and methods

2.1. Materials

Imidazole, Trizma acid (Tris) and its base, NaCl, protease inhibitor tablets EDTA (ethylenediaminetetraacetic acid)-free, Ni^{2+}-resin, TSP (3-(trimethylsilyl)propionic-2,2,3,3-d_4 acid sodium salt), DMSO (di-methyl sulfoxide), d_{12}-Tris acid and Amicon centrifugal devices with a molecular weight cut-off of 3 kDa were from Merck (Madrid, Spain; or Paris, France). Ampicillin and isopropyl-β-D-1-thiogalactopyranoside were obtained from Apollo Scientific (Stockport, UK). Triton X-100, and the sodium-dodecyl-sulfate protein marker (PAGEmark Tricolor) were from VWR (Barcelona, Spain). SAA was purchased from Eurodiagnostico, SL (Madrid, Spain). The rest of the materials were of analytical grade. Water was deionized and purified on a Millipore system (double distilled water).

2.2. Protein expression and purification

Wild-type NUPR1 was produced and purified from transformed BL21 (DE3) *E. coli* strain (Merck, Madrid, Spain) grown in Luria-Bertani broth medium as previously described [4]. For the ^{15}N-labeled wild-type NUPR1 the procedure was the same as in rich medium, but we used minimal medium supplemented with 1 g/L of $^{15}NH_4Cl$ [8] to grow the transformed BL21 (DE3) *E. coli* strain. The wild-type NUPR1 concentrations were obtained from the absorbance at 280 nm, by using the values for model compounds [30], and considering the presence of the two tyrosines in its sequence (Tyr30 and Tyr36).

The mutant T68Q of NUPR1 was expressed and purified from BL21 (DE3) *E. coli* strain as described [7]. The mutant concentration was determined as that of the wild-type protein.

The stock solutions of SAA used for the *in vitro* and cell-based experiments were prepared by dissolving a corresponding amount of powder to yield a stock solution of 7.2 mM (usually in a volume of 1–2 mL). For *in vitro* experiments the solvent was 100 % double-distilled water and for the in cell-based assays, the solvent used was 100 % DMSO.

2.3. Fluorescence titration experiments

A Cary Varian spectrofluorometer (Agilent, Santa Clara, CA, USA), interfaced with a Peltier unit, was used to collect fluorescence spectra. Samples were excited at 280 nm and the spectra were acquired between 300 and 400 nm. The bandwidth was 1 nm; the slit widths for excitation and emission were 5 nm. The fluorescence experiments were carried out at 25 °C in buffer Tris at 50 mM concentration (pH 7.8). In all experiments, a 1-cm pathlength cell (Hellma, GmbH & Co, Mülheim, Germany) was used.

For the titration between SAA and wild-type NUPR1, increasing amounts of SAA, in the concentration range 0–30 μM, were added to a solution with a fixed concentration of wild-type NUPR1 (5 μM). The samples were prepared 2 h before running the experiments. In all cases, the appropriate blank-corrections were made by subtracting the signal obtained with the corresponding amounts of isolated SAA by using KaleidaGraph (Synergy software, Reading, PA, USA). Spectra were corrected for inner-filter effects during fluorescence excitation [31]. The

titration was repeated twice, by using new samples; variations in the results of the two experiments for each SAA concentration were lower than 10 %.

The dissociation constant of the SAA/wild-type NUPR1 complex, K_d, was calculated by fitting the binding isotherm constructed by plotting the observed fluorescence change as a function of SAA concentration to a general binding model, explicitly considering protein depletion due to binding [32,33]:

$$F = F_0 + \frac{\Delta F_{max}}{2[NUPR1]_T}\left(([SAA]_T + [NUPR1]_T + K_d) - \sqrt{(([SAA]_T + [NUPR1]_T + K_d)^2 - 4[SAA]_T[NUPR1]_T}\right) \quad (1)$$

where F is the measured fluorescence at any particular concentration of SAA, after subtraction of the spectrum of a sample containing the same concentration of SAA (*i.e.*, F is the differential, or difference fluorescence); ΔF_{max} is the largest change in the fluorescence of SAA when all molecules were forming the complex, compared to the fluorescence of isolated wild-type NUPR1; F_0 is the fluorescence intensity when no SAA was added; $[NUPR1]_T$ is the constant, total concentration of wild-type NUPR1 (5.0 μM); and, $[SAA]_T$ is that of SAA, which was varied during the titration. Fitting to Eq. (1) was carried out by using KaleidaGraph.

Titration experiments with the NUPR1 mutant T68Q were carried out in a similar fashion and in the same range of molecule concentrations; data fitting was carried out with Eq. (1) as well. Experiments with the mutant were also repeated twice.

2.4. Isothermal titration calorimetry (ITC)

The interaction of wild-type NUPR1 and SAA was evaluated by using ITC with a VP-ITC instrument (MicroCal, Northampton, MA, USA) at 25 °C. The sample cell was loaded with wild-type NUPR1 at a concentration of 90 μM, whereas the syringe contained SAA at a concentration of 450 μM. Experiments were performed in buffer Tris at 10 mM concentration (pH 7.6), and 75 mM of NaCl.

A series of 19 injections with a 15-μL volume of SAA solutions were added sequentially to the sample cell after 420 s spacing with a stirring speed of 307 rpm. To correct for the heat developed by the dilution effect, an independent experiment was performed where the same ligand solution was injected into the calorimetric cell loaded with buffer. After correction for the heat of dilution, the thermodynamic parameters of binding were fitted to a single-site model to estimate the association constant, K_a (and therefore, to obtain also K_d); the stoichiometry of binding, n; and, the interaction enthalpy, ΔH. Data analysis was carried out employing the software package Origin 7.0 provided by MicroCal (Northampton, MA, USA).

2.5. Nuclear magnetic resonance (NMR)

The NMR experiments to measure the interaction between ^{15}N-labeled wild-type NUPR1 and SAA were performed at 20 °C, pH 7.5 (deuterated Tris buffer at concentration 50 mM, no correction was done for the isotopic effect), on a Bruker Avance II DRX-500 spectrometer (Bruker, Karlsruhe, Germany) equipped with a triple-resonance probe and z gradients. The protein assignment is deposited at BMRB (Biomagnetic Resonance Bank), at pH 4.5 (BMRB number: 19364 [8]); chemical shifts were extrapolated for the use under our conditions. All spectra were referenced to external TSP, as previously described [34].

The 2D ^{1}H,^{15}N-heteronuclear single-quantum coherence (HSQC) spectra [35] were acquired either for isolated ^{15}N-labeled wild-type NUPR1 (80 μM) or, alternatively, in the presence of 300 μM of SAA. Frequency discrimination in the indirect dimensions was achieved by using the echo/antiecho-TPPI (time proportional phase increment) method. The spectra were acquired with 1024 points in the ^{1}H dimension, 128 points in the ^{15}N dimension, and 200 scans. The carrier of the ^{1}H dimension was set at 5.00 ppm, and that of ^{15}N was set at 120 ppm. The spectral widths used were 12 ppm and 35 ppm in the ^{1}H and ^{15}N dimensions, respectively. Water signal was suppressed with the WATERGATE sequence [36]. Data were zero-filled to double the number of original points in both dimensions, apodized with shifted squared sine-bell functions in the two dimensions, and Fourier transformed with the program TopSpin 2.1 (Bruker, Karlsruhe, Germany). We measured the intensity of each isolated cross-peak by using the same program. The relative intensities of each cross-peak were calculated by using the intensity value of each cross-peak divided by the intensity value of the cross-peak corresponding to Gly1. We provided the relative intensity of each cross-peak with respect to the cross-peak of this residue (which is at the N terminus of the protein) in each spectrum, because the receiver gain of the HSQC spectra can change between the two experiments (in the absence and in the presence of SAA), and the value of the intensities of all residues can be modified consequently. Therefore, having an "internal" cross-peak as reference, which appears under both set of conditions (Section 3.1), was necessary, and this relative intensity allowed the comparison between the two acquired HSQC spectra.

2.6. Molecular docking simulations

The molecular docking of SAA to wild-type NUPR1 was modeled by using DiffDock [37], a powerful algorithm that simulates a diffusion process over the manifold of poses of the guest compound. This methodology, although circumventing the impracticability of applying other more accurate simulations techniques to study IDPs/ligand complexes, still relies on the availability of physically-realistic protein conformations. Therefore, the docking simulations were performed on eight structures extracted from a previous, experimentally-validated molecular dynamics (MD) of wild-type NUPR1 alone [38,39].

In brief, the structure of wild-type NUPR1 was built in an extended conformation and then collapsed in an MD run performed with the GROMACS package [40] for 40 ns in the isobaric-isothermal ensemble at standard temperature and pressure (reference values of 26.85 °C and 10^5 Pa, respectively). The AMBER ff99SB-ILDN force field [41] was used for wild-type NUPR1, and the standard TIP3P model [42] for water. Due to the spontaneous compaction of the wild-type NUPR1 conformation during the MD run, eight protein structures with decreasing radius of gyration (from 4.8 to 2.0 nm, at steps of 0.4 nm) were obtained at different simulation times (about 0.7, 1.0, 1.7, 6.4, 12.1, 19.5, 30.6, and 32.2 ns, respectively).

We previously reported that protein structures obtained with such MD runs correctly reproduce the electrostatic properties of NUPR1 chain [38], can mimic the dynamics of the capture mechanism of this protein in the presence of a ligand [39], and can be used as molecular hosts in a docking screening to successfully identify binders of NUPR1 [12].

The docking simulations were performed on the eight MD structures in a completely blind fashion, considering the whole protein surface. The calculations were carried out with default parameters (20 inference steps, 40 samples, and no final step noise), as previously described [43,44]. The best 10 docking poses were considered in each run, although in a few cases the less favorable poses were excluded because they were not bound to the protein as judged by visual inspection.

2.7. Cell lines

MIA PaCa-2 and Panc-1 cell lines were obtained from the American Type Culture Collection (ATCC) and cultured in Dulbecco's modified Eagle's medium (DMEM) (Gibco, ThermoFisher, Paris, France) supplemented with 10 % fetal bovine serum (FBS) (Biosera) at 37 °C and 5 % CO_2. Panc-1 NUPR1 KO cell line was developed in our laboratory through CRISPR/Cas9 technology and was cultured in DMEM supplemented with 10 % of FBS [45].

Human pancreatic stellate cell lines (hPSCs) were gifted from Pilar Navarro's laboratory (IIBB, Barcelona, Spain) and they were cultured in

DMEM-F12 (Gibco, ThermoFisher, Paris, France) supplemented with 10 % FBS. These cell lines were also cultured at 37 °C and with 5 % CO_2.

2.8. Proliferation assays

Five thousand cells were plated in 96-well plates and incubated overnight to let them attach to the plate. Next day, the cells were treated with increasing concentrations of SAA (0.01–100 μM) for 72 h. Cell viability was determined by employing PrestoBlue™ Cell Viability Reagent for 2 h. Then, the fluorescence of the supernatant was monitored by using the plate reader Tristar LB941. Cell viability was calculated as a percentage *versus* untreated cells. All the experiments were performed in triplicate.

2.9. Immunofluorescence

Cells were pleated in 24-well plates on glass coverslips at a 100,000 cells per well. Next day, cells were pre-treated with 20 μM SAA for 5 h prior the addition of the SGs formation inductor arsenate (at a concentration of 500 μM) for 1 h. Then, cells were washed and fixed with 4 % paraformaldehyde. After permeabilization with 0.2 % Triton X-100 and blocking, coverslips were incubated with primary antibodies anti-G3BP (1:200, Abcam ab56574, where G3BP is the Ras GTPase-activating protein-binding protein), anti-NUPR1 (1:200, homemade) or anti-TIA-1 (1:200, ThermoFisher PA5–18699, where TIA-1 stands for T-cell intracellular antigen protein 1) for 1.5 h. The secondary antibodies employed were, respectively, AlexaFluor647 donkey anti-mouse, AlexaFluor546 donkey anti-rabbit and AlexaFluor488 donkey anti-goat at dilution 1:500 for 1 h. Image were acquired by using a Zeiss Axio Imager Z2 microscope apotome (× 63 magnification lens).

2.10. Statistical analyses

Statistical analyses for the cell-based assays were conducted by using one-way ANOVA. The results were expressed as the mean ± SD (standard deviation) of at least three independent experiments. A *p*-value < 0.05 was regarded as statistically significant.

3. Results

3.1. In vitro binding of SAA to NUPR1 in the low micromolar range

We tested whether wild-type NUPR1 interacted with SAA *in vitro*, by using fluorescence, ITC and NMR. With the first two techniques we obtained a quantitative measurement of the thermodynamic parameters governing the binding, whereas NMR provided information about the preferences in the binding location of SAA to the protein.

The fluorescence spectrum of isolated wild-type NUPR1, due to the presence of its two tyrosine residues (Tyr30 and Tyr36), had a maximum at ~308 nm after excitation at 280 nm. In the presence of growing amounts of SAA, the corresponding spectra showed a decrease of intensity, but there were no changes in the maximum wavelength of the spectra. We observed that SAA did not show a fluorescence spectrum upon excitation at 280 nm but rather, it had fluorescent, after excitation at 370 nm.

We carried out fluorescence titrations to quantitatively measure the binding affinity, by keeping constant the concentration of wild-type NUPR1 and increasing the concentration of SAA. The results yielded a dissociation constant of 10 ± 2 μM (Fig. 1A). These findings suggest that Tyr30 and/or Tyr36 (the sole fluorescent residues in the protein) were involved in the binding to SAA. We also used Job's plots to characterize the binding of the two molecules, following standard procedures [46–49]. The intersection of the two lines (Fig. 1A, inset), representing the corrected fluorescence at different [SAA]/[NUPR1] rates, was 1.8 ± 0.9, which is an estimate of the stoichiometry of the complex. We also carried out fluorescence titrations with the T68Q mutant of NUPR1 and SAA (Fig. S1); the results suggest that the affinity (9 ± 2 μM) was the same as that of the wild-type species (10 ± 2 μM). Then, removal of this key residue at the second hot-spot was not enough to suppress the binding, which still occurred through the aromatic region of the protein,

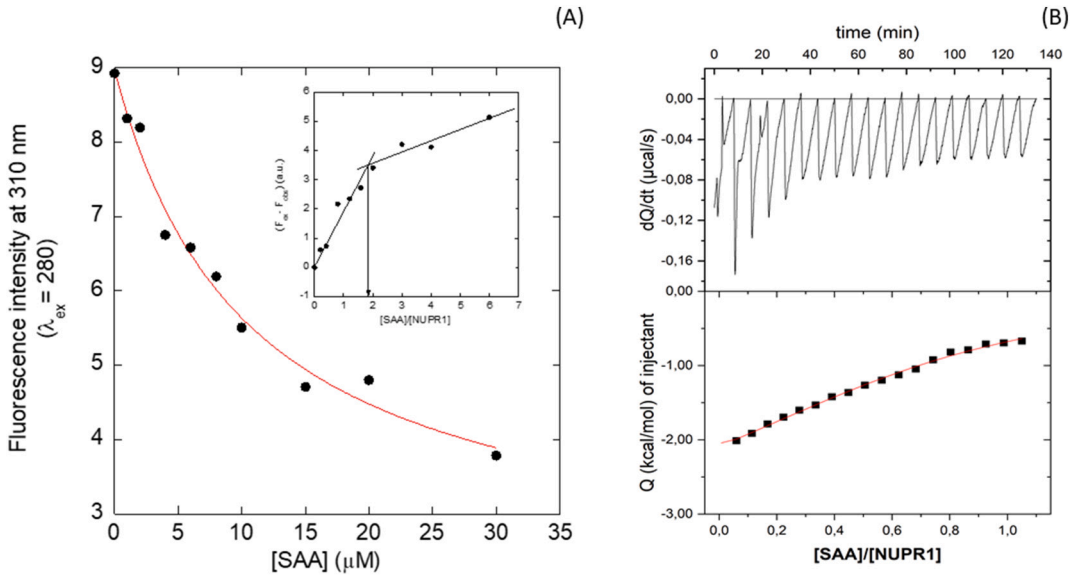

Fig. 1. Quantitative determination of the binding of SAA to wild-type NUPR1 monitored by different biophysical probes. (A) Titration curve monitoring the changes in the fluorescence at 310 nm when SAA was added to a fixed amount of wild-type NUPR1. The fluorescence intensity on the y-axis is the relative signal after removal of the corresponding blank. The line through the data is the fitting to Eq. (1). (Inset) Stoichiometry of the binding of SAA to wild-type NUPR1 monitored by using a Job's plot of the fluorescence titration. The difference $F_{exp} - F_{obs}$ (where F_{exp} is the sum of the corresponding fluorescence of the two isolated molecules, SAA and wild-type NUPR1, and F_{obs} is the measured fluorescence at 330 nm) is plotted *versus* the concentration ratio of the two biomolecules. The arrow indicates the intersection point between the two lines. (B) Calorimetric titrations of SAA with wild-type NUPR1. Upper panel show the thermograms (thermal power as a function of time) and lower panel show the binding isotherms (ligand-normalized heat effects *per* injection as a function of the molar ratio in the calorimetric cell). The lower panel was obtained after subtracting the dilution effect of SAA from the titration thermogram. The continuous line corresponds to the fitting curve according to a single ligand binding site interaction model.

i.e., the other protein hot-spot. Unfortunately, we were not able to successfully express in amounts large enough for our biophysical studies, the NUPR1 mutant modified at the other hot-spot of NUPR1, namely A33Q, neither the double mutant A33Q/T68Q [7].

We used ITC to determine the enthalpy and the entropy of the binding reaction for the wild-type species (Fig. 1B). The dissociation constant, K_d for the interaction of wild-type NUPR1 with SAA was 39 ± 5 μM, accompanied by a large enthalpic contribution of −3.3 ± 0.2 kcal mol^{-1}, and an entropic one of 9.2 ± 0.3 cal mol^{-1} $deg.^{-1}$. The *n* parameter (provided as [SAA]/[NUPR1]) was 0.72 ± 0.02, which was different to that obtained by the Job's plot in fluorescence (Fig. 1A inset).

Next, we used NMR to determine which residues were intervening in the binding to SAA and whether wild-type NUPR1 remained disordered upon binding to the stilbenoid, as it happens in its binding to other molecules [5–8,12,19,50]. When an excess of SAA was added to wild-type NUPR1, we observed a general decrease in the intensity of all the signals in the NMR spectra (Fig. 2); none of the lingering cross-peaks did show a change in chemical shifts, when compared to those measured in the isolated protein, indicating that wild-type NUPR1 remained disordered upon binding to SAA. Among the residues which could still be observed in the presence of SAA (Figs. 2 and S2) were: Gly1, Glu18, Tyr30, Ala33, His34 and Thr46. However, the largest variations in the relative intensity (with respect to Gly1 in each spectrum) between the two spectra – greater than one-third from the value in the spectrum with wild-type NUPR1 in isolation – were occurring at: Thr3, Ser23(Asn53), Ser27, Leu29, Tyr30, Ser31(Ser35), His34, Gly38, Ala50, Thr68 and Arg82 (amino acids within parentheses correspond to signal overlapping of the two cross-peaks). That is, the region with the largest number of residues with the most important variations in the relative intensities of the cross-peaks was that around the two aromatic residues of wild-type NUPR1: Tyr30 and Tyr36 (confirming the fluorescence results, Fig. 1A). Residue Thr68, belonging to the other hot-spot of wild-type NUPR1, showed the largest variation in the relative intensity between the two spectra (in the absence and in the presence of SAA). Then, the changes in the NMR spectra involved residues close, or belonging to, the two hot-spots of wild-type NUPR1, as it happens when it binds to other molecules [5–8,12,19,50]. The fact that there were some cross-peaks broadened beyond detection in the presence of SAA, whereas others were still observed – although with a lower intensity when compared to the same cross-peaks in the spectrum of the isolated wild-type NUPR1 – indicated that there were certain regions of wild-type NUPR1 that were preferentially bound to SAA. Furthermore, the finding that some signals disappeared when SAA was present suggested that there might be a slow-to-medium conformational exchange between the free- and SAA-bound- NUPR1 states. Then, taken together, all these findings argue against a non-specificity of the binding, as there are some amino acids which are more affected by the binding while others do not.

Overall, the biophysical probes indicate that *in vitro* binding of SAA to wild-type NUPR1 was in the low micromolar affinity, and with a stoichiometry between one and two SAA molecules *per* protein molecule.

3.2. The disordered complex NUPR1/SAA had conformational preferences

Molecular docking simulations were used to further study the association of SAA to NUPR1 at atomic detail. To this end, we employed the algorithm DiffDock [37], which uses a diffusion generative model based on deep learning to predict the binding of small molecules to a host protein. The docking hosts were eight structures extracted from an MD of NUPR1 alone [39], with radius of gyrations in the range 2.0–4.8 nm. Although not covering the whole thermodynamic ensemble of NUPR1 in solution, this set of structures modeled the protein at different degrees of compaction.

We note that state-of-the-art predictors based on neural networks fail to produce accurate structures for IDPs. As an example, AlphaFold [51] provides a prediction (entry: O60356) that: (1) is a single structure, whereas an ensemble of NUPR1 conformations with different compaction degree are present in solution, as suggested by our NMR studies on relaxation dynamics in the nanosecond-to-picosecond time regime [52]; (2) possesses many long helical regions, whereas in reality NUPR1 has 0 % secondary structure; (3) shows low confidence (pLDDT <70, where pLDDT stands for the predicted local distance difference test) in the unstructured parts, which are the only protein regions that might be correct. MD simulation predates machine learning algorithms in reproducing the conformation of small well-folded proteins [53]. For IDPs, although having the tendency to produce a single over-compact structure on the long run [54], MD samples multiple and physically accessible

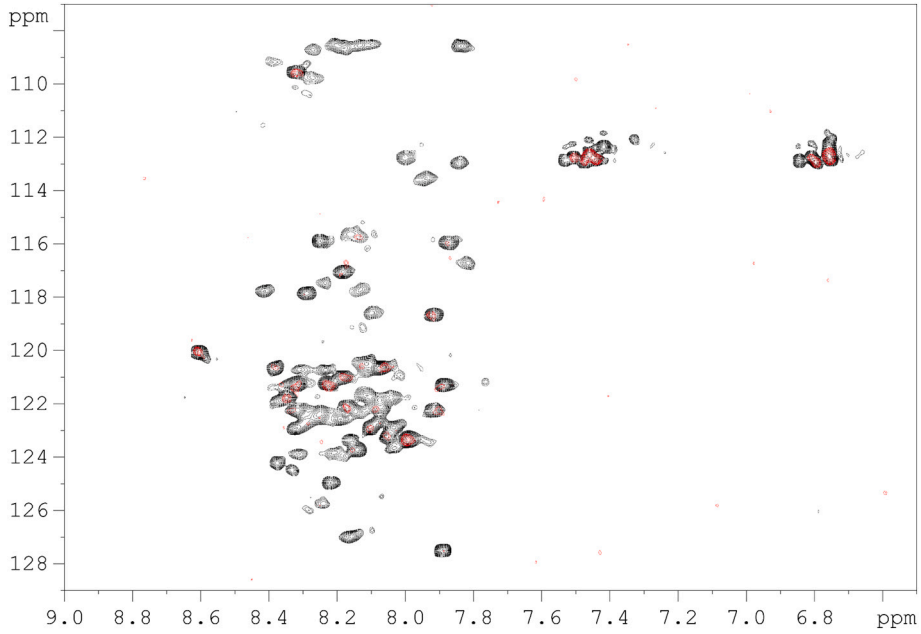

Fig. 2. 2D ^{1}H-^{15}N HSQC NMR spectra of wild-type NUPR1 with or without SAA. The 2D ^{1}H-^{15}N HSQC NMR spectra of wild-type NUPR1 (at 80 μM concentration) in the absence (black lines), and in the presence of SAA, at 300 μM of concentration (red lines). The same lower contour level was used for both spectra.

protein conformations at shorter timescales, which can be conveniently used for molecular docking simulations.

The snapshots reported in Fig. 3 show the results obtained in the docking calculations. Although the docking poses obtained were very different from one snapshot to another, the overall picture that emerges was quite clear: there were two main binding locations of SAA on NUPR1, one encompassing the only two fluorescent residues Tyr30 and Tyr36 (evident in the accumulation of docking poses in Fig. 3B, G, and H), and the other one in-between His62 and Thr68 (more visible in Fig. 3A, C, D, E, and F). At least one docking pose was found close to either Tyr30 and Tyr36 in all the NUPR1 structures (pinpointing towards the importance of that region in the binding to SAA, as suggested by the fluorescent results with the wild-type and the T68Q mutant), and a few other isolated docking poses were occasionally found in other different locations.

These findings are in excellent agreement with both the fluorescence and NMR data at our disposal, as well as with the stoichiometry of the complex predicted by both fluorescence and ITC. In fact, it is worth to note that the two binding locations (Tyr30/Tyr36 and His62/Thr68) can coexist (and then, they increase the stoichiometry of the SAA/NUPR1 complex, as detected in the fluorescence experiments (Fig. 1A inset)), except when the protein structure is very collapsed (such as in Fig. 3H), when they merged into a single cluster of binding poses. The reason they may appear alternative to each other is that, for each simulation snapshot, the docking algorithm focuses mostly on one of the two locations when either of them is more favorable compared to the other.

In summary, our blind docking simulations, performed on MD structures spanning the conformations of NUPR1 at different values of gyration radius, suggested that there were two main binding locations of SAA on the protein. These locations correspond to the hot-spots of NUPR1, traditionally indicated as the '30s' and '60s' along the protein sequence [6,7,15], and which correspond to the two regions of slightly higher hydrophobicity of the protein [12]. The binding mechanism suggested by the docking calculations does not rely on either the host (NUPR1) or the guest (SAA) possessing a well-defined structure in the binding, neither requires a binding stoichiometry corresponding to an integer number.

3.3. Evaluating SAA effect in cell-based assays

The inhibition of NUPR1 has a deleterious effect on cancer cells, as it has been shown in previous studies [12,15,45]. Having shown *in vitro* and *in silico* that SAA bound to the hot-spot regions of wild-type NUPR1, we aimed to investigate whether this molecule could efficiently target NUPR1 in cell-based assays in pancreatic cancer cells. We first evaluated the effect of SAA treatment on the pancreatic cancer cell lines MIA PaCa-2 and Panc-1, obtaining IC_{50} values of 21.2 and 36.9 μM, respectively (Fig. 4A), which are close to the value obtained by ITC for the wild-type protein (Fig. 1B).

Additionally, we also tested the compound on hPSCs to investigate whether the cytotoxic effect of SAA observed in tumoral cells was also observed in non-malignant or mutated cells (Fig. 4A). We clearly observed that SAA did not show any cytotoxic effect on hPSCs. Only at the highest tested dose of SAA, a noticeable drop in the hPSCs viability was noticed. Therefore, we can conclude that these findings reveal that the effect of SAA was cell-dependent.

We have recently described wild-type NUPR1 as an essential component of SGs in pancreatic cancer cells [17]. To determine whether SAA was also capable of preventing SGs formation, where NUPR1 intervenes, MIA PaCa-2 cell lines were pre-treated with 20 μM of the stilbenoid for 5 h, and then challenged with the well-known SG inducer arsenate (at a concentration of 500 μM) for 1 h. Immunofluorescence with the use of several SG markers showed a drastic reduction in SG-positive cells following SAA treatment (Fig. 4B, C), revealing its action on these molecular condensates. However, at this stage, we cannot rule out that the disruption of SGs formation could be due not only to interaction of SAA with NUPR1 at its hot-spots, but, alternatively, to other possible mechanisms (such as the anti-oxidant action of SAA, observed with other redox compounds [31], or even with the presence of arsenate).

Finally, to assess whether the observed cellular effects of SAA were due to its interaction with NUPR1, we compared the impact of SAA on cell viability in NUPR1-deficient cell lines (Panc-1 NUPR1-KO) *versus* NUPR1-expressing cell lines (Panc-1 WT). We found no differences in sensitivity to SAA in the absence or presence of NUPR1, indicating that the cytotoxic effect detected above may be independent of NUPR1

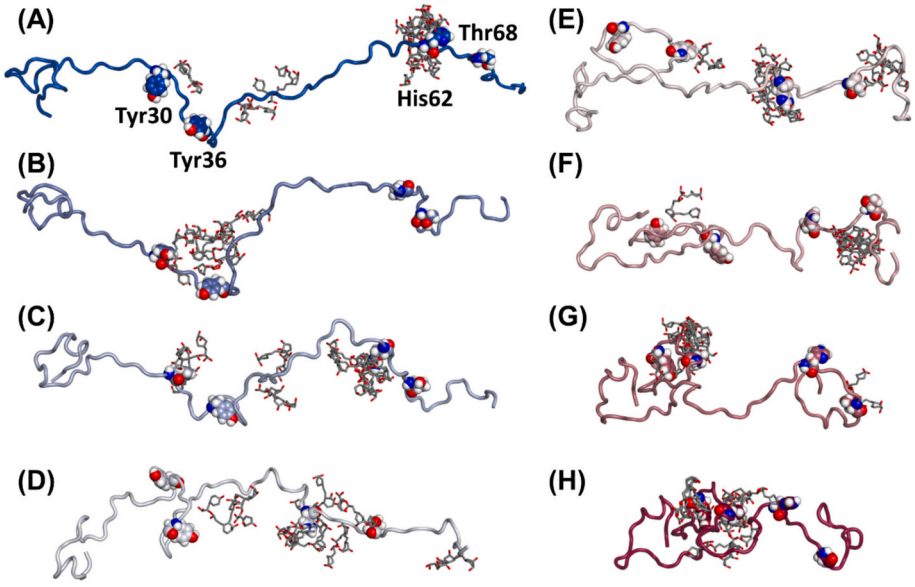

Fig. 3. Molecular docking simulations of SAA bound to wild-type NUPR1 at different degrees of compaction. Up to ten docking poses of SAA are bound for each NUPR1 structure at decreasing radius of gyration, in steps of 0.4 nm: (A) 4.8 nm, (B) 4.4 nm, (C) 4.0 nm, (D) 3.6 nm, (E) 3.2 nm, (F) 2.8 nm, (G) 2.4 nm, and (H) 2.0 nm. In all protein structures the N terminus is on the left and the C terminus on the right. Residues Tyr30/Tyr36 and His62/Thr68, which are conventionally delimiting the protein hot-spots in the '30s' and '60s' along the protein sequence, are explicitly represented in all structures, and labeled in the sole conformation at 4.8 nm.

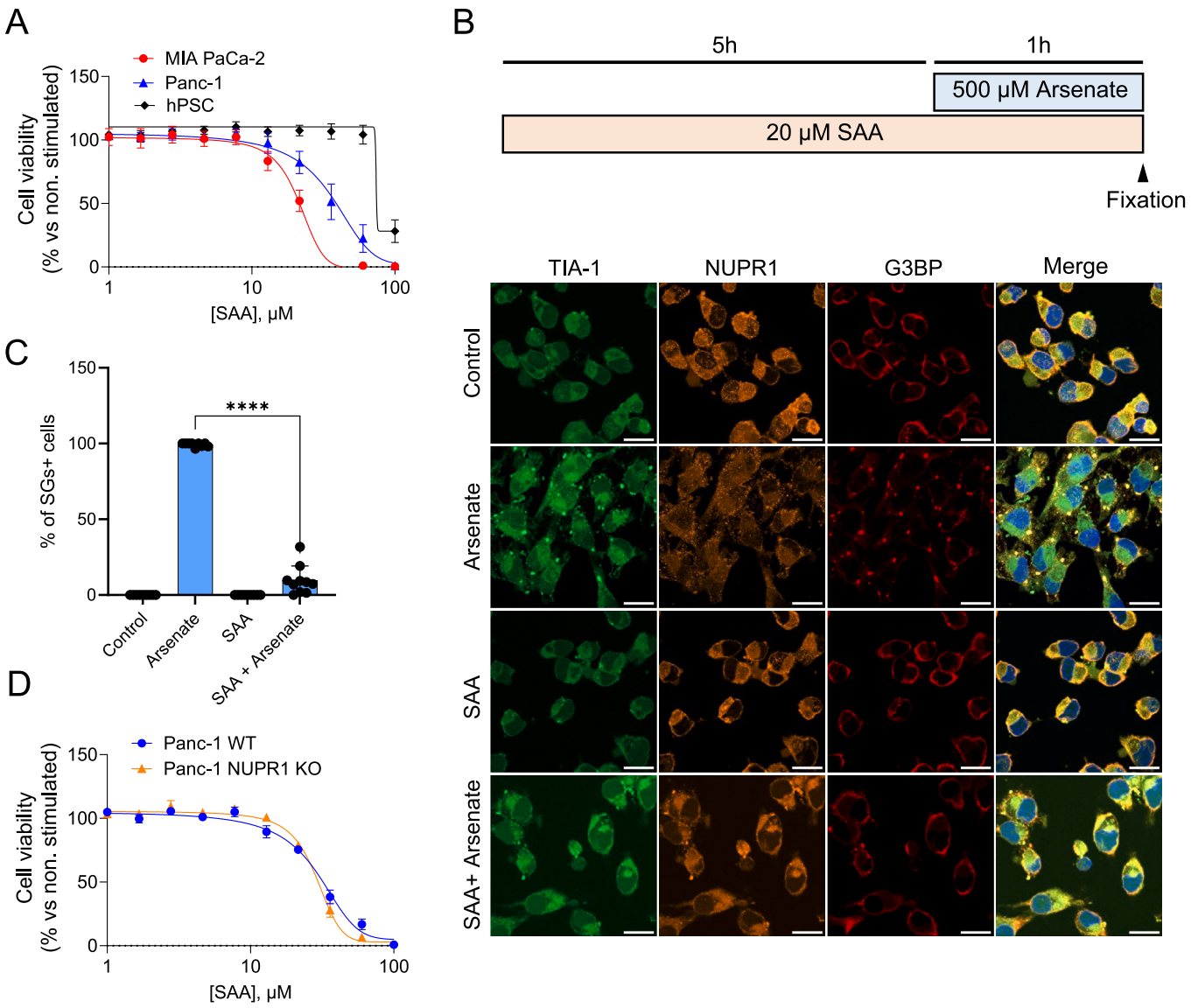

Fig. 4. Effect of SAA in the cell-based assays. (A) Cell viability assay upon SAA treatment for 72 h in pancreatic cancer cell lines MIA PaCa-2, Panc-1 and in human pancreatic stellate cells (hPSCs). The value represents the percentage of cell viability compared to untreated cells ($n = 3$). (B) SAA treatment inhibited SGs formation induced by arsenate. To induce SGs, MIA PaCa-2 cells were treated with 500 μM arsenate for 1 h. To test the effect of SAA to counteract SGs formation, cells were pre-treated with 20 μM of the stilbenoid for 5 h prior the addition of SGs inductor. Representative images of cells after treatments staining with anti-TIA1, anti-NUPR1 and anti-G3BP antibodies. Scale bar represents 20 μm. (C) Quantification of SGs positive MIA PaCa-2 cells upon treatments. The graph represents the percentage of cells with SGs (mean ± SD, n = 3). (D) Cell viability upon SAA treatment in Panc-1 WT or Panc-1 NUPR1 KO cells. The value represents the percentage of cell viability compared to untreated cells (n = 3). (SAA, salvianolic acid, ****, *p*-value <0,0001).

expression in the cell (Fig. 4D).

4. Discussion

4.1. SAA was bound to NUPR1

Trying to search for new lead compounds targeting diseases, natural products have unique advantages in terms of availability and scaffold diversity. *Salvia miltiorrhiza* (also known as Chinese sage or Danshen) is one of the most important herbal medicinal drugs in TCM, as it is used to treat several blood disorders [55]. Salvianolic acids are very abundant in the plants and, together with tanshinones (lipophilic, diterpenic quinones), they are the main active principles of herbal drugs. They show protective roles in central neuronal injuries and degeneration, probably acting on the levels of reactive oxygen species (ROS); in fact, SAA is a potent scavenger of ROS during cardiovascular injury, inhibiting the adherence of leukocytes to endothelial cells [56]. Furthermore, there is evidence of the protective role of salvianolic acids in several cardiovascular diseases, liver fibrosis, hepatic failure and osteoporosis [55,57,58].

SAA can exert its anticancer activity through inhibition of cell proliferation, migration, and invasion, induction of apoptosis, and modulation of critical signaling pathways like PI3K (Phosphoinositide 3-kinase protein)/Akt (protein kinase B), mTORC (mammalian target of rapamycin kinase), and Wnt/β-catenin [59,60]. This raises an advantage over other treatments, as SAA could potentially circumvent the limitations of conventional monotherapies by impacting on a broad range of molecular targets by using of drug cocktails. Along this line, recent proteomic and chemo-proteomic analyses have further revealed that SAA could covalently bind to numerous cellular proteins, including the mTORC1 subunit Raptor, and thereby interfering with important tumor-promoting pathways [61]. SAA has also been shown to inhibit some of

the isoforms of human carbonic anhydrase [62], and it binds to the active site of matrix metalloproteinase-9 (MMP9), exerting anti-inflammatory effects [63].

In this work, we have studied the effect of the interaction of SAA with NUPR1, which is a multifunctional protein with an interactome including dozens of other protein partners [64]. As many other IDPs, NUPR1 is heavily involved in cell regulation and signaling, including key tumor pathways in PDAC and several other cancer types. We have shown that SAA was bound to NUPR1 in a specific way *in vitro*, as if the association were non-specific, we should not observe in the NMR spectrum that cross-peaks of NUPR1 showed different behavior in their variation of the intensities in the presence of this compound. Furthermore, our docking simulations showed that there were two main binding regions of SAA, corresponding to the two hot-spot regions of NUPR1 for the binding of other molecular partners [12,15], therefore indicating that the binding was specific. The affinity constant of SAA for wild-type NUPR1 (~20 μM), as determined by ITC and fluorescence, was similar to that measured for other synthetic compounds, either identified from a large library, or specifically designed to target this protein [12,15]. However, the mutant protein at Thr68 (T68Q) also showed the same affinity for SAA as indicated by fluorescence (Fig. S1). These results contrast with what is observed for the binding of the natural protein partners of NUPR1 or during the SG formation, where the use of this mutant leads to absence of protein binding or to the appearance of SGs [12,15]. Then, it seems that SAA should have a slightly higher affinity for the region around Tyr30 and Tyr36 (the first hot-spot), than for that around the Thr68 polypeptide patch, in agreement with the results found in some poses of the molecular docking results (Section 3.2). Overall, and independently which of the two hot-spots of NUPR1 SAA was mainly aiming to, these findings are noteworthy, because identifying good binders *in vitro* targeting IDPs is generally challenging, due to the highly hydrophobic and flexible character of these proteins. Moreover, these results also show that we have found a binder for NUPR1 which seems to have a certain preference for one of the two hot-spots. In our case, the fact that SAA is a stilbenoid adds an additional point of interest, as it further expands the chemical space of potential inhibitors of NUPR1 (and more generally of IDPs) towards the use of natural compounds, or even its modification in future chemical campaigns targeting NUPR1; that is, using SAA as a lead compound to develop others, which in the cells could have this IDP as the main target.

Our results in the cell-based assays further demonstrated that SAA had a clear cytotoxic effect on the pancreatic tumor cell lines MIA PaCa-2 and Panc-1. However, this effect did not appear to depend on a possible interaction with NUPR1, as suggested by the negative results with Panc-1 NUPR1-KO cell lines. At an IC_{50} dose, the compound showed no cytotoxic effect on hPSCs. A decrease in the hPSC viability was only observed at high doses (100 μM) (Fig. 4A). The antioxidant capacity of SAA and its cytotoxic effect on hPSCs have been demonstrated [65]. However, such cytotoxic effects in some cells do not invalidate the possible use of SAA as an anticancer drug, since other well-known protein targets of this compound (such as MMP9 or carbonic anhydrase) could explain the cytotoxic effect in the cells used in this work. In addition, SAA has also antioxidant activities [26,65] which could, instead, underlie the cytotoxicity observed in some of the assayed cells. Now, we miss an explanation of why SAA – while binding NUPR1 at the same hot-spots as other compounds and natural partners, with a similar affinity *in vitro* – yet does not have this protein as its main target in the experiments with cells. The NMR results can provide a hint about the binding of SAA to NUPR1, and its inability to target primarily such protein. Upon addition of SAA, all the NMR signals showed a decrease of their intensities (Fig. 2), whereas in the case of other organic compounds, only a small number of residues – namely, those close to, or belonging to, the hot-spots – showed a small variation of the intensities of their cross-peaks [12–16]. Then, it seems that in the dynamic conformational space NUPR1 is exploring, a larger number of residues intervene in the binding of the stilbenoid, allowing the binding to one hot-spot if the other is crippled (as it happened for the mutant T68Q, Fig. S1). Then, as there is a balance between target function and drug affinity, it seems that there is as well a compromise between the NUPR1 function and the number of residues, outside the NUPR1 hot-spots, involved in anchoring the compound to the polypeptide chain. In future studies, using SAA as a lead compound to be optimized, we may modify the alkyl groups of the compound while keeping its organic scaffold, but we should take in consideration that any chemical variation should yield a modified stilbenoid which must have the same affinity as SAA *in vitro*, or improve it, but it should not affect many of the cross-peaks in the HSQC spectrum of NUPR1.

4.2. SAA and the hampering of the SGs formation

We next proceeded to study the SGs formation triggered by the presence of NUPR1 with the aim of checking whether the presence of the stilbenoid would make any difference. In an expected turn of screw, SAA effectively counteracted SGs formation, triggered by wild-type NUPR1, following arsenate treatment. SGs are membrane-less organelles that assemble in the cytoplasm in response to cellular stress [66]. Furthermore, our docking simulations suggested that SAA could target concomitantly both hot-spots of NUPR1 (Fig. 3), explaining the different stoichiometry found by fluorescence and ITC (Fig. 1); the anchoring to the two hot-spots by different moieties of the stilbenoid could explain why SAA is successful in hampering the SGs formation triggered by NUPR1. However, it is important to pinpoint that, although we have shown that: (i) SAA binds to NUPR1 *in vitro* and *in silico* through its hot-spots (Figs. 1, 2 and 3); and (ii) NUPR1 is necessary for SGs formation [17], we do not have any unambiguous proof that inhibition of SGs formation is exclusively modulated by the presence of NUPR1 within the cell.

The functions of SGs range from protecting and storing mRNA to regulating signaling pathways. In pancreatic cancer cells specifically, SGs have been described as protective structures that help cells survive chemotherapy and acquire treatment resistance [17,67]. Advanced glycation end-products are capable of disrupting LLPS triggered by Galectin-3 and integrin α5β1 [68], and synthetic peptides can hamper the SG formation triggered by G3BP1 [69], a protein with a key role in RNA metabolism and stress response [70]. Furthermore, LLPS promoted by α-synuclein, a protein involved in several neurodegenerative diseases, is hampered by synthetic zwitterionic compounds [71]. This has led to a growing interest in identifying small molecules that regulate SG formation, since synthetic or natural compounds can modulate growing and chemoresistance of cancer cells. NUPR1, due to its intrinsically disordered nature, has been identified as a component of SGs in pancreatic cancer cells, and NUPR1 inhibition by the compound ZZW-115, which binds to the same hot-spots as SAA, is known to disrupt SG assembly [17]. We do not know the exact mechanism by which SAA hampered SGs formation in our experiments with NUPR1; that disruption could be related to: (i) SAA potent ROS scavenger activity (which could be shown in the presence of arsenate, used in facilitating SGs formation); or, alternatively, (ii) its high promiscuity in binding to other proteins, as SAA does interact with carbonic anhydrase [62] and MMP9 [63]. At this stage, however, we cannot exclude the possibility that, under stress conditions where NUPR1 levels are very high, SAA might bind not only to this protein, but also, and concomitantly, to others with a higher affinity than that reported here for NUPR1. Yet, even in that alternative scenario, SAA will be one of the first natural compounds capable of hindering SG formation by binding to the hot-spots of an IDP.

5. Conclusions

We have shown that SAA was capable of binding to NUPR1, an IDP, with an affinity like that measured for other compounds capable of binding this protein, and exploiting the same hot-spots along its amino acid sequence. These findings do not only introduce a new molecular

scaffold that could be improved to inhibit PPIs of this protein for a therapeutic purpose, but also extend the possibility to target IDPs by using natural compounds, including herbal medicinal compounds or extracts that have been already used for a long time in TCM. However, future improvements of the SAA alkyl chains, or even of the core region of its scaffold, should consider how the affinity must be improved without modifying in excess the binding to the protein hot spots, without interacting with many residues outside of those regions.

Although SAA showed a cytotoxic effect on several pancreatic cancer lines in the cell-based assays, such outcome does not seem to be directly related to its ability to bind NUPR1 within the cell. However, SAA could hamper the SGs formation within the cells where NUPR1 was also implicated, although further studies will be necessary to determine the specific cellular pathways involved in those processes. The outcome of such future research may be of help to suggest new therapeutic alternatives for pancreatic cancer, and other hard-to-treat tumors.

CRediT authorship contribution statement

María Gabriela Álvarez-Rodríguez: Writing – review & editing, Investigation, Formal analysis. **Matías Estaras:** Writing – review & editing, Writing – original draft, Methodology, Investigation, Formal analysis, Conceptualization. **Felipe Hornos:** Writing – review & editing, Writing – original draft, Methodology, Investigation, Formal analysis. **Bruno Rizzuti:** Writing – review & editing, Writing – original draft, Project administration, Methodology, Investigation, Funding acquisition, Formal analysis, Conceptualization. **Patricia Santofimia-Castaño:** Writing – review & editing, Methodology, Investigation, Formal analysis. **Juan L. Iovanna:** Writing – review & editing, Writing – original draft, Methodology, Funding acquisition, Conceptualization. **José L. Neira:** Writing – review & editing, Writing – original draft, Project administration, Methodology, Investigation, Funding acquisition, Formal analysis, Conceptualization.

Declaration of competing interest

The authors declare no competing interests.

Acknowledgements

This research was funded by HORIZON European Union [EXPLORA GA n° 101181841 to JLN, FH and MGAR] and by Next Generation EU program, Italian PNNR, Mission 4, Component 2, Investment 1.5, "Innovation Ecosystems" project Tech4You, "Technologies for Climate Change Adaptation and Quality of Life Improvement" [CUP B83C22003980006 to BR], Spoke 3. ME was granted with a postdoctoral fellowship from ARC Foundation.

The funders had no role in the study design, data collection and analysis, decision to publish, or preparation of the manuscript.

We thank Dr. Chris Johnson (MRC-LMB, Cambridge, UK) for helpful discussions and advice about the ITC measurements. We thank Dr. Pilar Navarro (IIBB, Barcelona, Spain) for the kind gift of hPSCs.

We thank the two anonymous reviewers for helpful suggestions of new experiments and improvements. We thank Prof. Timir Tripathi for handling the manuscript.

Appendix A. Supplementary data

There are two figures in the Supplementary Material: the fluorescence titration of NUPR1 mutant T68Q with SAA (Fig. S1); and the rows from the 2D ^{1}H,^{15}N-HSQC spectra (in the absence and in the presence of SAA) corresponding to the ^{15}N chemical shifts of Leu29, Tyr30 (together with Thr68) and Ala33 for wild-type NUPR1 (Fig. S2). Supplementary data to this article can be found online at https://doi.org/10.1016/j.ijbiomac.2025.149435.

Data availability

All the materials are available upon reasonable request from the corresponding authors.

References

[1] S. Goruppi, J.L. Iovanna, Stress-inducible protein p8 is involved in several physiological and pathological processes, J. Biol. Chem. 285 (2010) 1577–1581, https://doi.org/10.1074/JBC.R109.080887.
[2] C.E. Cano, T. Hamidi, M.J. Sandi, J.L. Iovanna, Nupr1: the Swiss-knife of cancer, J. Cell. Physiol. 226 (2011) 1439–1443, https://doi.org/10.1002/JCP.22324.
[3] M.J. Sandi, T. Hamidi, C. Malicet, C. Cano, C. Loncle, A. Pierres, J.C. Dagorn, J. L. Iovanna, p8 expression controls pancreatic cancer cell migration, invasion, adhesion, and tumorigenesis, J. Cell. Physiol. 226 (2011) 3442–3451, https://doi.org/10.1002/JCP.22702.
[4] J.A. Encinar, G.V. Mallo, C. Mizyrycki, L. Giono, J.M. González-Ros, M. Rico, E. Cánepa, S. Moreno, J.L. Neira, J.L. Iovanna, Human p8 is a HMG-I/Y-like protein with DNA binding activity enhanced by phosphorylation, J. Biol. Chem. 276 (2001) 2742–2751, https://doi.org/10.1074/JBC.M008594200.
[5] P. Santofimia-Castaño, B. Rizzuti, A.L. Pey, M.E. Fárez-Vidal, J.L. Iovanna, J. L. Neira, Intrinsically disordered protein NUPR1 binds to the armadillo-repeat domain of Plakophilin 1, Int. J. Biol. Macromol. 170 (2021) 549–560, https://doi.org/10.1016/J.IJBIOMAC.2020.12.193.
[6] M. Estaras, B. Rizzuti, A.M. Giudici, J.A. Poveda, J.L. Iovanna, P. Santofimia-Castaño, J.L. Neira, The intrinsically disordered protein NUPR1 binds to phospholipids, Protein Sci. 34 (2025), https://doi.org/10.1002/PRO.70236.
[7] P. Santofimia-Castaño, B. Rizzuti, Á.L. Pey, P. Soubeyran, M. Vidal, R. Urrutia, J. L. Iovanna, J.L. Neira, Intrinsically disordered chromatin protein NUPR1 binds to the C-terminal region of Polycomb RING1B, Proc. Natl. Acad. Sci. USA 114 (2017) E6332–E6341, https://doi.org/10.1073/PNAS.1619932114.
[8] D. Aguado-Llera, T. Hamidi, R. Doménech, D. Pantoja-Uceda, M. Gironella, J. Santoro, A. Velázquez-Campoy, J.L. Neira, J.L. Iovanna, Deciphering the binding between Nupr1 and MSL1 and their DNA-repairing activity, PLoS One 8 (2013), https://doi.org/10.1371/journal.pone.0078101.
[9] G.V. Mallo, F. Fiedler, E.L. Calvo, E.M. Ortiz, S. Vasseur, V. Keim, J. Morisset, J. L. Iovanna, Cloning and expression of the rat p8 cDNA, a new gene activated in pancreas during the acute phase of pancreatitis, pancreatic development, and regeneration, and which promotes cellular growth, J. Biol. Chem. 272 (1997) 32360–32369, https://doi.org/10.1074/jbc.272.51.32360.
[10] S.B. Su, Y. Motoo, J.L. Iovanna, M.J. Xie, H. Mouri, K. Ohtsubo, Y. Yamaguchi, H. Watanabe, T. Okai, F. Matsubara, N. Sawabu, Expression of p8 in human pancreatic cancer, Clin. Cancer Res. 7 (2001) 309–313.
[11] P. Santofimia-Castaño, B. Rizzuti, Y. Xia, O. Abian, L. Peng, A. Velázquez-Campoy, J.L. Neira, J. Iovanna, Targeting intrinsically disordered proteins involved in cancer, Cell. Mol. Life Sci. 77 (2020) 1695–1707, https://doi.org/10.1007/S00018-019-03347-3.
[12] J.L. Neira, J. Bintz, M. Arruebo, B. Rizzuti, T. Bonacci, S. Vega, A. Lanas, A. Velázquez-Campoy, J.L. Iovanna, O. Abián, Identification of a drug targeting an intrinsically disordered protein involved in pancreatic adenocarcinoma, Sci. Rep. 7 (2017), https://doi.org/10.1038/SREP39732.
[13] B. Rizzuti, W. Lan, P. Santofimia-Castaño, Z. Zhou, A. Velázquez-Campoy, O. Abián, L. Peng, J.L. Neira, Y. Xia, J.L. Iovanna, Design of inhibitors of the intrinsically disordered protein nupr1: balance between drug affinity and target function, Biomolecules 11 (2021), https://doi.org/10.3390/BIOM11101453.
[14] P. Santofimia-Castaño, Y. Xia, L. Peng, A. Velázquez-Campoy, O. Abián, W. Lan, G. Lomberk, R. Urrutia, B. Rizzuti, P. Soubeyran, J.L. Neira, J. Iovanna, Targeting the stress-induced protein NUPR1 to treat pancreatic adenocarcinoma, Cells 8 (2019), https://doi.org/10.3390/CELLS8111453.
[15] X. Liu, A. Jimenez-Alesanco, Z. Li, B. Rizzuti, J.L. Neira, M. Estaras, L. Peng, E. Chuluyan, J. Garona, F. Gottardo, A. Velazquez-Campoy, Y. Xia, O. Abian, P. Santofimia-Castaño, J. Iovanna, Development of an efficient NUPR1 inhibitor with anticancer activity, Sci. Rep. 14 (2024) 1–20, https://doi.org/10.1038/s41598-024-79340-z, 2024 14:1.
[16] P. Santofimia-Castaño, Y. Xia, W. Lan, Z. Zhou, C. Huang, L. Peng, P. Soubeyran, A. Velázquez-Campoy, O. Abián, B. Rizzuti, J.L. Neira, J. Iovanna, Ligand-based design identifies a potent NUPR1 inhibitor exerting anticancer activity via necroptosis, J. Clin. Invest. 129 (2019) 2500–2513, https://doi.org/10.1172/JCI127223.
[17] P. Santofimia-Castaño, N. Fraunhoffer, X. Liu, I.F. Bessone, M.P. di Magliano, S. Audebert, L. Camoin, M. Estaras, M. Brenière, M. Modesti, G. Lomberk, R. Urrutia, P. Soubeyran, J.L. Neira, J. Iovanna, Targeting NUPR1-dependent stress granules formation to induce synthetic lethality in KrasG12D-driven tumors, EMBO Mol. Med. 16 (2024) 475–505, https://doi.org/10.1038/S44321-024-00032-2.
[18] S.Y. Choi, Y.S. Koh, S.H. Jo, Inhibition of human ether-a-go-go-related gene K+ channel and IKr of guinea pig cardiomyocytes by antipsychotic drug trifluoperazine, J. Pharmacol. Exp. Ther. 313 (2005) 888–895, https://doi.org/10.1124/JPET.104.080853.
[19] L.F. Peña, M. Estaras, P. González-Andrés, C. Díez-Poza, B. Rizzuti, O. Abian, A. Velazquez-Campoy, J.L. Iovanna, P. Santofimia-Castaño, J.L. Neira, A. Barbero, Organosilicon molecules bind to the intrinsically disordered protein NUPR1 by clamping its hot-spots, Arch. Biochem. Biophys. 771 (2025) 110513, https://doi.org/10.1016/j.abb.2025.110513.

[20] Y. Liu, C. Fang, J. Luo, C. Gong, L. Wang, S. Zhu, Traditional Chinese medicine for cancer treatment, Am. J. Chin. Med. 52 (2024) 583–604, https://doi.org/10.1142/S0192415X24500253.
[21] L. Zhou, Z. Zuo, M.S.S. Chow, Danshen: An overview of its chemistry, pharmacology, pharmacokinetics, and clinical use, J. Clin. Pharmacol. 45 (2005) 1345–1359, https://doi.org/10.1177/0091270005282630.
[22] J.A. Rothwell, V. Knaze, R. Zamora-Ros, Polyphenols: dietary assessment and role in the prevention of cancers, Curr. Opin. Clin. Nutr. Metab. Care 20 (2017) 512–521, https://doi.org/10.1097/MCO.0000000000000424.
[23] Y. Zhou, J. Zheng, Y. Li, D.P. Xu, S. Li, Y.M. Chen, H. Bin Li, Natural polyphenols for prevention and treatment of cancer, Nutrients 8 (2016), https://doi.org/10.3390/NU8080515.
[24] S. Ma, D. Zhang, H. Lou, L. Sun, J. Ji, Evaluation of the anti-inflammatory activities of tanshinones isolated from Salvia miltiorrhiza var. Alba roots in THP-1 macrophages, J. Ethnopharmacol. 188 (2016) 193–199, https://doi.org/10.1016/j.jep.2016.05.018.
[25] C. Spatafora, C. Tringali, Natural-derived polyphenols as potential anticancer agents, Anti Cancer Agents Med. Chem. 12 (2012) 902–918, https://doi.org/10.2174/187152012802649996.
[26] C.Y. Su, Q.L. Ming, K. Rahman, T. Han, L.P. Qin, Salvia miltiorrhiza: traditional medicinal uses, chemistry, and pharmacology, Chin. J. Nat. Med. 13 (2015) 163–182, https://doi.org/10.1016/S1875-5364(15)30002-9.
[27] T. Qin, A. Rasul, A. Sarfraz, I. Sarfraz, G. Hussain, H. Anwar, A. Riaz, S. Liu, W. Wei, J. Li, X. Li, Salvianolic acid A & B: potential cytotoxic polyphenols in battle against cancer via targeting multiple signaling pathways, Int. J. Biol. Sci. 15 (2019) 2256–2264, https://doi.org/10.7150/IJBS.37467.
[28] L. Xiang, Y. Wang, S. Liu, B. Liu, X. Jin, X. Cao, Targeting protein aggregates with natural products: an optional strategy for neurodegenerative diseases, Int. J. Mol. Sci. 24 (2023) 11275, https://doi.org/10.3390/IJMS241411275, 2023, Vol. 24, Page 11275.
[29] B. Ahmad, L.J. Lapidus, Curcumin prevents aggregation in α-synuclein by increasing reconfiguration rate, J. Biol. Chem. 287 (2012) 9193–9199, https://doi.org/10.1074/JBC.M111.325548.
[30] S.C. Gill, P.H. von Hippel, Calculation of protein extinction coefficients from amino acid sequence data, Anal. Biochem. 182 (1989) 319–326, https://doi.org/10.1016/0003-2697(89)90602-7.
[31] B. Birdsall, R.W. King, M.R. Wheeler, C.A. Lewis, S.R. Goode, R.B. Dunlap, G.C. K. Roberts, Correction for light absorption in fluorescence studies of protein-ligand interactions, Anal. Biochem. 132 (1983) 353–361, https://doi.org/10.1016/0003-2697(83)90020-9.
[32] C.A. Royer, S.F. Scarlata, Chapter 5 fluorescence approaches to quantifying biomolecular interactions, Methods Enzymol. 450 (2008) 79–106, https://doi.org/10.1016/S0076-6879(08)03405-8.
[33] D. Beckett, Measurement and analysis of equilibrium binding titrations: a beginner's guide, Methods Enzymol. 488 (2011) 1–16, https://doi.org/10.1016/B978-0-12-381268-1.00001-X.
[34] J. Cavanagh, W.J. Fairbrother, A.G. Palmer, N.J. Skelton, Protein NMR Spectroscopy: Principles and Practice, 2nd edition, 2007.
[35] G. Bodenhausen, D.J. Ruben, Natural abundance nitrogen-15 NMR by enhanced heteronuclear spectroscopy, Chem. Phys. Lett. 69 (1980) 185–189, https://doi.org/10.1016/0009-2614(80)80041-8.
[36] M. Piotto, V. Saudek, V. Sklenář, Gradient-tailored excitation for single-quantum NMR spectroscopy of aqueous solutions, J. Biomol. NMR 2 (1992) 661–665, https://doi.org/10.1007/BF02192855.
[37] G. Corso, H. Stärk, B. Jing, R. Barzilay, T. Jaakkola, DiffDock: Diffusion Steps, Twists, and Turns for Molecular Docking. https://arxiv.org/abs/2210.01776v2, 2022. (Accessed 8 September 2024).
[38] J.L. Neira, B. Rizzuti, J.L. Iovanna, Determinants of the pK<inf>a</inf> values of ionizable residues in an intrinsically disordered protein, Arch. Biochem. Biophys. 598 (2016), https://doi.org/10.1016/j.abb.2016.03.034.
[39] P. Santofimia-Castaño, B. Rizzuti, O. Abián, A. Velázquez-Campoy, J.L. Iovanna, J. L. Neira, Amphipathic helical peptides hamper protein-protein interactions of the intrinsically disordered chromatin nuclear protein 1 (NUPR1), Biochim. Biophys. Acta Gen. Subj. 1862 (2018), https://doi.org/10.1016/j.bbagen.2018.03.009.
[40] S. Pronk, S. Páll, R. Schulz, P. Larsson, P. Bjelkmar, R. Apostolov, M.R. Shirts, J. C. Smith, P.M. Kasson, D. Van Der Spoel, B. Hess, E. Lindahl, GROMACS 4.5: a high-throughput and highly parallel open source molecular simulation toolkit, Bioinformatics 29 (2013) 845–854, https://doi.org/10.1093/BIOINFORMATICS/BTT055.
[41] K. Lindorff-Larsen, S. Piana, K. Palmo, P. Maragakis, J.L. Klepeis, R.O. Dror, D. E. Shaw, Improved side-chain torsion potentials for the Amber ff99SB protein force field, Proteins Struct. Funct. Bioinform. 78 (2010) 1950–1958, https://doi.org/10.1002/PROT.22711.
[42] W.L. Jorgensen, J. Chandrasekhar, J.D. Madura, R.W. Impey, M.L. Klein, Comparison of simple potential functions for simulating liquid water, J. Chem. Phys. 79 (1983) 926–935, https://doi.org/10.1063/1.445869.
[43] J.L. Neira, B. Rizzuti, M. Palomino-Schätzlein, V. Rejas, O. Abian, A. Velazquez-Campoy, Citrullination at the N-terminal region of MDM2 by the PADI4 enzyme, Protein Sci. 34 (2025), https://doi.org/10.1002/PRO.70033.
[44] S. Araujo-Abad, B. García-Peñarrubia, A.M. Giudici, J.L. Neira, B. Rizzuti, C. de Juan Romero, J.A. Poveda, The citrullinating enzyme PADI4 binds to lipids: identification of new target interactions for cancer therapy, J. Mol. Biol. 437 (2025), https://doi.org/10.1016/j.jmb.2025.169297.
[45] P. Santofimia-Castaño, W. Lan, J. Bintz, O. Gayet, A. Carrier, G. Lomberk, J. L. Neira, A. González, R. Urrutia, P. Soubeyran, J. Iovanna, Inactivation of NUPR1 promotes cell death by coupling ER-stress responses with necrosis, Sci. Rep. 8 (2018), https://doi.org/10.1038/s41598-018-35020-3.
[46] J.L. Neira, F.J. Florencio, M.I. Muro-Pastor, The isolated, twenty-three-residue-long, N-terminal region of the glutamine synthetase inactivating factor binds to its target, Biophys. Chem. 228 (2017) 1–9, https://doi.org/10.1016/j.bpc.2017.05.017.
[47] J.L. Neira, B. Rizzuti, O. Abian, A. Velazquez-Campoy, Isolated auto-citrullinated regions of PADI4 associate to the intact protein without altering their disordered conformation, Biophys. Chem. 312 (2024), https://doi.org/10.1016/j.bpc.2024.107288.
[48] L. Saelices, C.V. Galmozzi, F.J. Florencio, M.I. Muro-Pastor, J.L. Neira, The inactivating factor of glutamine synthetase IF17 Is an intrinsically disordered protein, which folds upon binding to its target, Biochemistry 50 (2011) 9767–9778, https://doi.org/10.1021/BI2009272/SUPPL_FILE/BI2009272_SI_001.PDF.
[49] D.E. Otzen, D.M.S. Lundvig, R. Wimmer, L.H. Nielsen, J.R. Pedersen, P.H. Jensen, p25α is flexible but natively folded and binds tubulin with oligomeric stoichiometry, Protein Sci. 14 (2005) 1396–1409, https://doi.org/10.1110/PS.041285605.
[50] S. Araujo-Abad, J.L. Neira, B. Rizzuti, P. García-Morales, C. de Juan Romero, P. Santofimia-Castaño, J. Iovanna, Intrinsically disordered chromatin protein NUPR1 binds to the enzyme PADI4, J. Mol. Biol. 435 (2023), https://doi.org/10.1016/J.JMB.2023.168033.
[51] M. Varadi, S. Anyango, M. Deshpande, S. Nair, C. Natassia, G. Yordanova, D. Yuan, O. Stroe, G. Wood, A. Laydon, A. Zídek, T. Green, K. Tunyasuvunakool, S. Petersen, J. Jumper, E. Clancy, R. Green, A. Vora, M. Lutfi, M. Figurnov, A. Cowie, N. Hobbs, P. Kohli, G. Kleywegt, E. Birney, D. Hassabis, S. Velankar, AlphaFold Protein Structure Database: massively expanding the structural coverage of protein-sequence space with high-accuracy models, Nucleic Acids Res. 50 (2022) D439–D444, https://doi.org/10.1093/NAR/GKAB1061.
[52] A. Bonucci, M. Palomino-Schätzlein, P. Malo de Molina, A. Arbe, R. Pierattelli, B. Rizzuti, J.L. Iovanna, J.L. Neira, Crowding effects on the structure and dynamics of the intrinsically disordered nuclear chromatin protein NUPR1, Front. Mol. Biosci. 8 (2021) 684622, https://doi.org/10.3389/FMOLB.2021.684622/BIBTEX.
[53] K. Lindorff-Larsen, S. Piana, R.O. Dror, D.E. Shaw, How fast-folding proteins fold, Science 334 (2011) 517–520, https://doi.org/10.1126/SCIENCE.1208351.
[54] F.N.K. Muhammedkutty, M. MacAinsh, H.X. Zhou, Atomistic molecular dynamics simulations of intrinsically disordered proteins, Curr. Opin. Struct. Biol. 92 (2025) 103029, https://doi.org/10.1016/J.SBI.2025.103029.
[55] L. Bonaccini, A. Karioti, M.C. Bergonzi, A.R. Bilia, Effects of Salvia miltiorrhiza on CNS neuronal injury and degeneration: a plausible complementary role of tanshinones and depsides, Planta Med. 81 (2015) 1003–1016, https://doi.org/10.1055/S-0035-1546196.
[56] W. Zhong, B. Sun, W. Gao, Y. Qin, H. Zhang, L. Huai, Y. Tang, Y. Liang, L. He, X. Zhang, H. Tao, S. Chen, W. Yang, L. Yang, Y. Liu, H. Liu, H. Zhou, T. Sun, C. Yang, Salvianolic acid A targeting the transgelin-actin complex to enhance vasoconstriction, EBioMedicine 37 (2018) 246–258, https://doi.org/10.1016/j.ebiom.2018.10.041.
[57] W.Y. Wu, Y.P. Wang, Pharmacological actions and therapeutic applications of Salvia miltiorrhiza depside salt and its active components, Acta Pharmacol. Sin. 33 (2012) 1119–1130, https://doi.org/10.1038/APS.2012.126.
[58] J.H.C. Ho, C.Y. Hong, Salvianolic acids: small compounds with multiple mechanisms for cardiovascular protection, J. Biomed. Sci. 18 (2011), https://doi.org/10.1186/1423-0127-18-30.
[59] T. Ye, R. Chen, Y. Zhou, J. Zhang, Z. Zhang, H. Wei, Y. Xu, Y. Wang, Y. Zhang, Salvianolic acid A (Sal A) suppresses malignant progression of glioma and enhances temozolomide (TMZ) sensitivity via repressing transgelin-2 (TAGLN2) mediated phosphatidylinositol-3-kinase (PI3K)/protein kinase B (Akt) pathway, Bioengineered 13 (2022) 11646–11655, https://doi.org/10.1080/21655979.2022.2070963.
[60] C.X. Li, Q. Xu, S.T. Jiang, D. Liu, C. Tang, W.L. Yang, Anticancer effects of salvianolic acid A through multiple signaling pathways (Review), Mol. Med. Rep. 32 (2025), https://doi.org/10.3892/MMR.2025.13541.
[61] M. Zheng, Y. Zhang, Y. Xu, Y. Han, Y. Wu, J. Kang, Chemoproteomics and phosphoproteomics profiling reveals salvianolic acid A as a covalent inhibitor of mTORC1, J. Proteome Res. 22 (2023) 2450–2459, https://doi.org/10.1021/ACS.JPROTEOME.3C00188/ASSET/IMAGES/LARGE/PR3C00188_0006.JPEG.
[62] A. Karioti, F. Carta, C.T. Supuran, Phenols and polyphenols as carbonic anhydrase inhibitors, Molecules 21 (2016) 1649, https://doi.org/10.3390/MOLECULES21121649, 2016, Vol. 21, Page 1649.
[63] B. Jiang, D. Li, Y. Deng, F. Teng, J. Chen, S. Xue, X. Kong, C. Luo, X. Shen, H. Jiang, F. Xu, W. Yang, J. Yin, Y. Wang, H. Chen, W. Wu, X. Liu, D. an Guo, Salvianolic acid A, a novel matrix metalloproteinase-9 inhibitor, prevents cardiac remodeling in spontaneously hypertensive rats, PLoS One 8 (2013), https://doi.org/10.1371/JOURNAL.PONE.0059621.
[64] W. Lan, P. Santofimia-Castaño, M. Swayden, Y. Xia, Z. Zhou, S. Audebert, L. Camoin, C. Huang, L. Peng, A. Jiménez-Alesanco, A. Velázquez-Campoy, O. Abián, G. Lomberk, R. Urrutia, B. Rizzuti, V. Geli, P. Soubeyran, J.L. Neira, J. Iovanna, ZZW-115-dependent inhibition of NUPR1 nuclear translocation sensitizes cancer cells to genotoxic agents, JCI Insight 5 (2020), https://doi.org/10.1172/JCI.INSIGHT.138117.
[65] M. Estaras, C. Ortiz-Placin, A. Castillejo-Rufo, M. Fernandez-Bermejo, G. Blanco, J. M. Mateos, D. Vara, P.L. Gonzalez-Cordero, S. Chamizo, D. Lopez, A. Rojas, I. Jaen, N. de Armas, G.M. Salido, J.L. Iovanna, P. Santofimia-Castaño, A. Gonzalez, Melatonin controls cell proliferation and modulates mitochondrial physiology in

pancreatic stellate cells, J. Physiol. Biochem. 79 (2023) 235–249, https://doi.org/10.1007/S13105-022-00930-4.
[66] Y. Jia, R. Jia, Z. Dai, J. Zhou, J. Ruan, W.J. Chng, Z. Cai, X. Zhang, Stress granules in cancer: adaptive dynamics and therapeutic implications, IScience 27 (2024), https://doi.org/10.1016/j.isci.2024.110359.
[67] F. Xing, Y. Qin, J. Xu, W. Wang, B. Zhang, Stress granules dynamics and promising functions in pancreatic cancer, Biochim. Biophys. Acta Rev. Cancer 1878 (2023), https://doi.org/10.1016/j.bbcan.2023.188885.
[68] Z. Zhang, Z. Zhao, X. Huang, L. Zhou, X. Jiang, H. Wu, C. Liu, K. Huang, J. Wen, Y. Liu, M.C. Miller, Z. Zhao, Z. He, Y. Wang, S. Liu, L. Huang, L. Yuan, R. Zeng, Z. Cen, A. Chen, Y. Chen, G. Zeng, W. Liu, X. Hong, M. Ren, L. Yan, Y. Zhang, D. Guan, X. Tian, W. Cai, G. Tai, K.H. Mayo, Y. Zhou, Z. Li, S. Chen, Galectin-3-integrin α5β1 phase separation disrupted by advanced glycation end-products impairs diabetic wound healing in rodents, Nat. Commun. 16 (2025) 7287, https://doi.org/10.1038/S41467-025-62320-W.
[69] C. Liu, K. Wu, H. Choi, H.L. Han, X. Zhang, J.L. Watson, G. Ahn, J.Z. Zhang, S. Shijo, L.L. Good, C.M. Fischer, A.K. Bera, A. Kang, E. Brackenbrough, B. Coventry, D.R. Hick, S. Qamar, X. Li, J. Decarreau, S.R. Gerben, W. Yang, I. Goreshnik, D. Vafeados, X. Wang, M. Lamb, A. Murray, S. Kenny, M.S. Bauer, A. N. Hoofnagle, P. Zhu, T.P.J. Knowles, D. Baker, Diffusing protein binders to intrinsically disordered proteins, Nature (2025), https://doi.org/10.1038/S41586-025-09248-9.
[70] P. Yang, C. Mathieu, R.M. Kolaitis, P. Zhang, J. Messing, U. Yurtsever, Z. Yang, J. Wu, Y. Li, Q. Pan, J. Yu, E.W. Martin, T. Mittag, H.J. Kim, J.P. Taylor, G3BP1 is a tunable switch that triggers phase separation to assemble stress granules, Cell 181 (2020) 325–345.e28, https://doi.org/10.1016/j.cell.2020.03.046.
[71] D. Sarkar, S. Roychowdhury, R. Jain, K. Chattopadhyay, B. Banerji, Small molecule modulators of α-synuclein phase separation, ACS Chem. Neurosci. (2025), https://doi.org/10.1021/ACSCHEMNEURO.5C00302.